Analyzing Mortar Baseplate Movement Using Differential Equations

Alexander Le*

Advisors: Dr. Maila Hallare†, Maj. A.J. Wallerstein‡

Abstract

Knowing baseplate kinematics during mortar fire allows for more accurate shelling during military operations. During mortar fire, ignition causes a rapid increase in barrel pressure, exerting a recoil force onto the baseplate and causing it to sink into the ground. This sinkage causes the barrel to move and fire shells slightly off trajectory. Accordingly, shells may miss their targets or hit unintentional ones. Using second-order linear differential equations, mortar kinematics was analyzed as an externally-forced spring-mass-damper system. Soil properties accounted for springiness and damping in this model, with recoil as the external forcing function. Simulations of the differential equations show that mortar movement was significantly minimized with larger baseplate area, and that launch angle did not significantly affect vertical sinkage. This project recommends that mortar baseplate area should be maximized to allow for more accurate artillery strikes.

1 Introduction

Mortars have historically served as a means for indirect fire. By launching at high angles (>45° elevation), mortars can strike targets hidden behind obstacles and terrain [3]. This proved useful during World War II, when American forces in France used mortars to fire over high buildings [15]. Modern mortars are made of a bipod (mount) with aiming mechanisms, a baseplate, and a barrel (cannon) [14]. Figure 1 shows how these mortars are assembled.

After aiming, mortar crews load a shell into the front of the barrel. The shell then slides downwards and reaches the firing pin located at the base of the barrel. This ignites the propellant and launches the shell outwards [9]. Ignition pressure acting onto the base of the barrel contributes to recoil forces, while pressure acting radially does not [13]. Recoil force is then transmitted into the ground through the baseplate. Mortars do not have built-in recoil-absorbing devices. After the projectile leaves, the mortar's inertia continues to push the baseplate deeper into the ground, as seen in Figure 2. At this point, the ground's reaction force is the only force acting on the mortar [3]. Mortar baseplates may be embedded into the soil such that the soil resists baseplate movement in all directions. The paper will proceed with this setup.

Effective mortar operations rely on rapid, precise fire [14]. During these operations, however, the baseplate will sink into the ground due to the recoil force. This baseplate sinkage causes the barrel to deviate from the original launch angle. These deviations are significant; at a 5,000 m range, a deviation of 1°can cause the shell to strike 80 m off-target [3]. Therefore, to increase strike accuracy, one must minimize baseplate movement during fire.

This paper is organized as follows. Section 2 describes the mortar-ground system in terms of differential equations, and determine the parameters required to solve it. Afterwards, Section 3 discusses how to solve the mortar system's differential equation and analyze its damping behavior. In Section 4, we establish the various soil, launch angle, and baseplate area conditions that our simulations will run. The exact simulation parameters are found in Appendix A. Then, we will proceed to discuss our results in Sections 5 and 6. Section 5 focuses on baseplate displacement and velocity, while Section 6 focuses on soil damping behavior under the various simulation conditions.

*United States Air Force Academy, c27alexander.le@afacademy.af.edu

†United States Air Force Academy, maila.hallare@afacademy.af.edu

‡United States Air Force Academy, austin.wallerstein@afacademy.af.edu

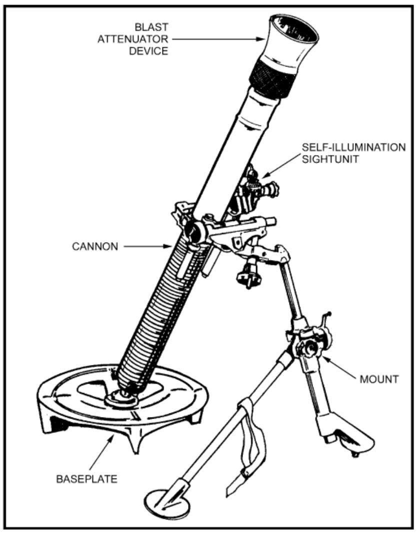

Figure 1: Mortars, including the M252 mortar pictured here, are assembled with a bipod, baseplate, and barrel. From [14].

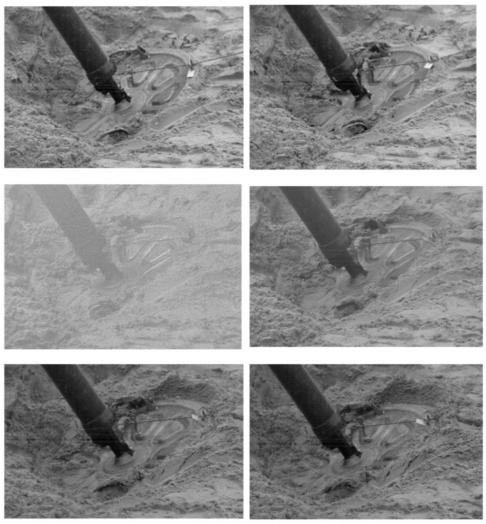

Figure 2: This high speed camera footage shows that mortar baseplates sink into the soil during firing. From [3].

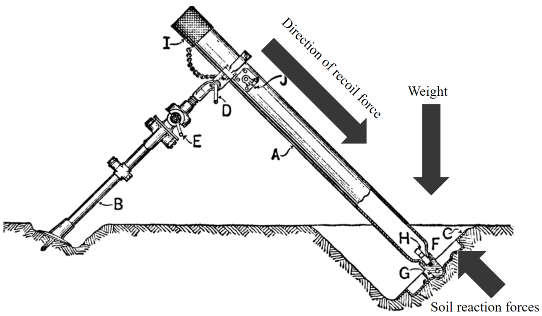

Figure 3: This mortar setup includes a bipod and aiming mechanisms (parts labeled B, E, D, J), a barrel (parts A, H, I), and a baseplate (parts C, F, G). From [8].

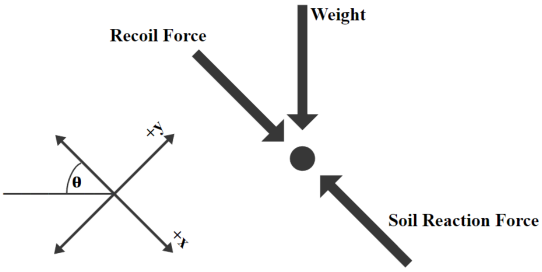

Figure 4: This is the free-body diagram for the mortar system, where θ is the launch angle.

The exact peak displacement, sinkage, and velocity values can be found in Appendix B. In Section 7, we summarize our findings, describe avenues for further research, and address the issues we encountered during the research process.

2 Mathematical Modeling

This section constructs a free-body diagram of the mortar-ground system and creates a differential equation describing it. Then, we calculate the recoil, soil, and mortar parameters required to solve the differential equation.

2.1 Free-Body Diagram

A diagram of a typical mortar setup and involved forces are illustrated in Figure 3. Let θ refer to the angle between flat ground and the barrel. Turning Figure 3 into a free-body diagram where the x-axis and the recoil force are parallel, one obtains Figure 4.

For mortars, the weight is negligible compared to recoil force. For example, the 35.3 kg L16A mortar launches 4.2 kg shells at a muzzle velocity of 225 m/s through a 1280 mm-long barrel [6]. Since the shell was at rest at the bottom of the barrel, one finds that the average recoil force is 83 kN. Meanwhile, the force of gravity on the mortar is 346 N. We see that gravity is negligible compared to recoil force, since 346 N/83 kN $\approx$ 0.004169. Hence, Figure 4 simplifies to Figure 5:

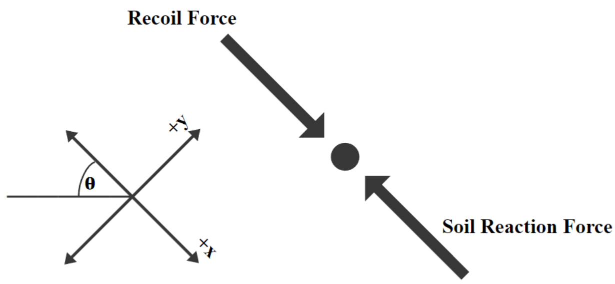

Figure 5: The force of weight can be considered negligible relative to recoil.

Soil properties are complex and highly variable. However, soil could be considered to have some springiness and damping. As the baseplate displaces deeper into the soil, it experiences increasing resistive force. Therefore, soil may be modeled as a spring that exerts a force with magnitude $kx(t)$, where k refers to the soil's spring constant and $x(t)$ refers to baseplate displacement. Soil is also viscous; as the baseplate moves through the soil, it experiences a resistive force proportional to its velocity. This means that soil may be modeled as a damper that exerts a force with magnitude $cv(t)$, where c refers to the soil damping properties and $v(t)$ refers to baseplate velocity. See Figure 6.

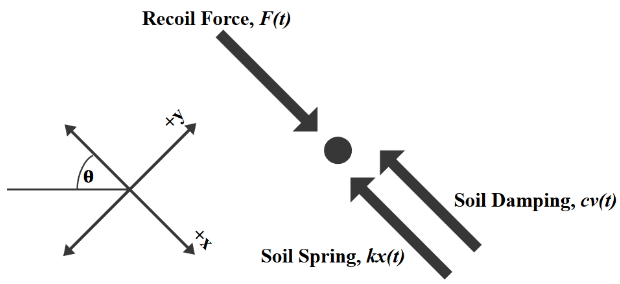

Figure 6: The forces involved in the mortar dynamics are recoil, soil spring force, and soil damping force.

We assume that soil spring and damping constants are proportional to contact area - doubling baseplate area doubles the amount of contact with soil springs and soil dampers. Additionally, we assume that the soil resistive forces directly oppose recoil force. From Figure 6, one obtains:

$$F(t) - cv(t) - kx(t) = ma(t). \tag{1}$$

Substituting velocity and acceleration for the first and second time derivatives of displacement and rearranging, we have:

$$mx''(t) + cx'(t) + kx(t) = F(t). \tag{2}$$

Observe that the equation is a linear, non-homogeneous, second-order differential equation. Next, we need to find the recoil, soil, and mortar values in order to conduct simulations.

2.2 Recoil Parameters

This subsection will consider how the recoil force varies over the course of the mortar's firing cycle. Pressure acting radially along the inner walls of the barrel does not contribute to recoil; any pressure exerted on a particular section of the wall is balanced by an equal pressure acting on a directly opposite section. Therefore, recoil force must be from pressure acting on the bottom of the barrel. This means that recoil force, $F(t)$, can be obtained by multiplying the barrel pressure over time, $p(t)$, by the area of the bottom of the barrel [13]. Plots showing how the barrel pressure changes over time are often referred to *pressure-time profiles*. Note that the internal diameter, d, of the barrel is often measured in millimeters; a 60-mm mortar has an internal barrel diameter of 60 mm. Here, $F(t)$ is modelled by:

$$F(t) = \frac{d^2}{4}\pi \cdot p(t). \tag{3}$$

Figure 7 describes the typical pressure-time profiles for mortars. From time t_0 to t_i, the flame spreads across the gunpowder grains. There is minimal pressure increase during this period. Then, from t_i to t_p, mortar pressure rapidly increases as the gunpowder ignites, reaching peak pressure at t_p. As the shell accelerates outwards (increasing the volume below the shell), barrel pressure drops from t_p to t_e. When the shell exits at t_e, barrel pressure continues to drop until it equalizes with atmospheric pressure at t_f.

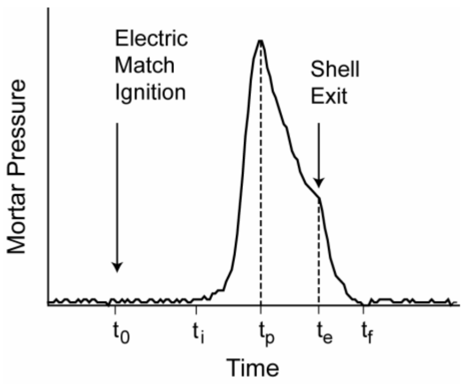

Figure 7: This diagram depicts barrel pressure over time during firing, from [13].

To approximate the mortar pressure profile $p(t)$, we proceed as follows. First, $t = 0$ will be defined as starting from t_i. The pressure rise from t_i to t_p will be approximated as an exponential growth, multiplied by a Heaviside function to ensure that the exponential growth only models pressure for the time period between t_i and t_p. The pressure decrease after t_p will be approximated as an exponential decay, multiplied by a Heaviside so that it only models pressure for the time period after t_p. Let C_1, C_2, k_1, and k_2 refer to parameters that control the exponential growth and decay approximations. Then one obtains:

$$p(t) = C_1 e^{k_1 t}(h(t) - h(t - t_p)) + C_2 e^{k_2 t}(h(t - t_p)). \tag{4}$$

Sources [3] and [12] provided barrel pressure-time plots for 60-mm and 120-mm mortars. These plots are shown in Figures 8 and 9. Plotting software (WebPlotDigitizer, [16]) was used to pull discrete data points from these plots[1].

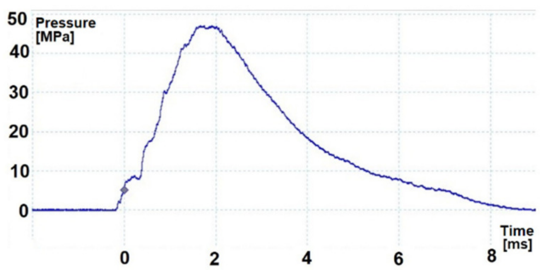

Figure 8: This is the pressure profile for a 60-mm mortar. From [3].

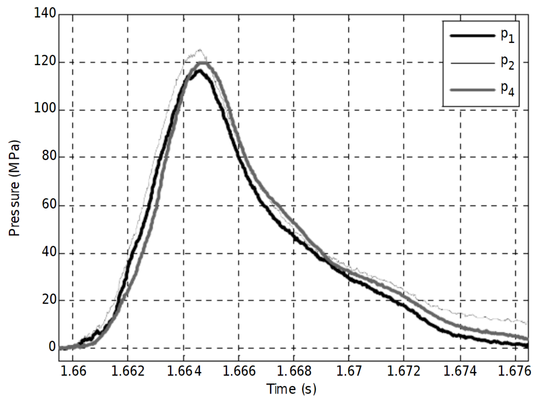

Figure 9: This is the pressure profile for a 120-mm mortar. p_1, p_2, p_4 refer to different barrel pressure estimates obtained during testing. From [12].

[1]WebPlotDigitizer works by finding the pixel location of a given point on a graph and comparing it to the axes of the graph

Note that equation (4) assumed that t_i was centered at $t = 0$. Because the original pressure-time data did *not* center t_i at $t = 0$, a calibration of the time-axis was done.

For the 60-mm pressure data, it was unclear exactly how much the original plot's time-axis needed to be shifted to center t_i at $t = 0$. To correctly shift, t_i was first identified using the original plot's time-axis. Using WebPlotDigitizer, t_i was found to be at $t = -0.0001889$. After exporting the pressure-time values into a spreadsheet, all time values were shifted leftwards by 0.0001889 seconds to center t_i at $t = 0$.

Regarding the pressure data for 120-mm mortars, reference [12] noted that p_1 and p_4 were slight underestimates of barrel pressure (with p_4 being slightly more accurate) and p_2 was a slight overestimate. We considered the actual barrel pressure to be the average between p_4 and p_2. For the 120-mm pressure data, WebPlotDigitizer was used to center t_i at the 1.66 second mark on the original pressure-time plot. After this calibration step, WebPlotDigitizer was used to read discrete pressure-time points off of the graph.

Pressure and time values for 60-mm and 120-mm mortars were then imported into MATLAB's curve-fitter program. Then, equation (4) was inputted as a custom equation to fit the pressure-time values. A summary of the results can be found in Table 1:

Parameters	60-mm mortar	120-mm mortar
C_1	$8.043 \cdot 10^6$	$11.23 \cdot 10^6$
C_2	$128.2 \cdot 10^6$	$406.5 \cdot 10^6$
k_1	1064	570.1
k_2	-457.3	-253.0
t_p	0.001889	0.004633
r^2	.9692	.9548

Table 1: These values are used in equation (4) to approximate barrel pressure.

Equation (3) was then used to convert these pressure-time equations into force-time equations. Thus, the recoil forces as a function of time are:

$$F(t) = 0.005685e^{(1064t)}(h(t) - h(t - 0.001889)) + 0.09061e^{(-457.3t)}(h(t - 0.001889)). \quad (5)$$

$$F(t) = 0.03174e^{(570.1t)}(h(t) - h(t - 0.004633)) + 1.149e^{(-253.0t)}(h(t - 0.004633)). \quad (6)$$

for 60-mm and 120-mm mortars, respectively

2.3 Soil Parameters

As mentioned previously, spring and damping coefficients are proportional to area. For a bridge with a total foundation area of $280\,\mathrm{m}^2$, Gharad and Sonparote estimated soil spring and damping coefficients [11]:

Table 3 Dynamic stiffness and dashpot values for different soil conditions

Description	Degree of freedom	Hard soil	Medium soil	Soft soil
Dynamic stiffness (kN/m)	$\tilde{K}_x$	4.59×10^6	1.79×10^6	6.46×10^5
	$\tilde{K}_y$	4.74×10^6	1.85×10^6	6.66×10^5
	$\tilde{K}_z$	5.98×10^6	2.33×10^6	8.40×10^5
	$\tilde{K}_{rx}$	3.32×10^7	1.30×10^7	4.66×10^6
	$\tilde{K}_{ry}$	5.78×10^7	2.26×10^7	8.13×10^6
	$\tilde{K}_t$	1.50×10^7	5.88×10^6	2.12×10^6
Dynamic damping (kN·s/m)	C_x	3.73×10^4	2.38×10^4	1.48×10^4
	C_y	3.73×10^4	2.38×10^4	1.48×10^4
	C_z	7.79×10^4	4.87×10^4	2.92×10^4
	C_{rx}	5.35×10^4	3.34×10^4	2.01×10^4
	C_{ry}	1.22×10^5	7.62×10^4	4.57×10^4
	C_t	1.54×10^4	9.65×10^3	5.79×10^3

Figure 10: This table, from [11], estimates soil spring and damping coefficients for a $280\,\mathrm{m}^2$ area.

K and C refer to the soil's spring and damping constants, respectively. The x and y subscripts refer to movement parallel to and lateral to their bridge model. The z subscript refers to vertical movement. To correct for the kilo- prefix and adjust to a $1\,\mathrm{m}^2$ area, all values were multiplied by

$\frac{1000}{280}$. For modeling purposes, K_h was taken to be the middle between K_x and K_y. C_h was taken to be the middle between C_x and C_y. The rx, ry, and t subscripts refer to rotational and torsional movement. These values were ignored as rotation and torsion is not of interest to this paper. Soil has numerous properties, but one can classify soils into "hard," "medium," and "soft" categories. For example, heavily compacted soil is likely rather "hard", clay soils could be classified as "medium", while loose peat soil is very "soft". Adjusting for a $1\,\mathrm{m}^2$ area, one obtains Table 2.

Soil Condition	Hard	Medium	Soft
K_h, N/m	$16.66 \cdot 10^6$	$6.500 \cdot 10^6$	$2.343 \cdot 10^6$
K_z, N/m	$21.36 \cdot 10^6$	$8.321 \cdot 10^6$	$3.000 \cdot 10^6$
C_h, N·s/m	$133.2 \cdot 10^3$	$85.00 \cdot 10^3$	$52.86 \cdot 10^3$
C_z, N·s/m	$278.2 \cdot 10^3$	$173.9 \cdot 10^3$	$104.3 \cdot 10^3$

Table 2: This table describes the soil spring and damping constants for a $1\,\mathrm{m}^2$ area.

To find K_h, K_z, C_h, and C_z for a particular baseplate area, that baseplate area (in m^2) was multiplied by the values in Table 2. The exact baseplate areas for 60-mm and 120-mm mortars are detailed in the next subsection.

Observe that these coefficients are slightly higher in the vertical direction[11]. This means that launch angle must be taken into consideration when calculating the net spring and net damping constants. Since the displacement has a vertical and horizontal component, the baseplate will experience a spring constant, K_n, that is a combination of the soil spring's vertical, K_z, and horizontal, K_h, constants (note that K_h and K_z have already been adjusted for that particular baseplate's area). With a launch angle of θ, the displacement x along the $+x$ axis will have a horizontal component $x\cos\theta$ and vertical component $x\sin\theta$. Calculating the horizontal spring force F_{s_h} and the vertical spring force F_{s_z}:

$$F_{s_h} = x\cos\theta \cdot K_h, F_{s_z} = x\sin\theta \cdot K_z,$$

Thus, the net spring force, F_{s_n} is:

$$F_{s_n} = \sqrt{F_{s_h}^2 + F_{z_h}^2}.$$

Let $F_{s_n} = x \cdot K_n$, where K_n is the net spring constant. Expanding and simplifying, one obtains:

$$K_n = \sqrt{(\cos\theta \cdot K_h)^2 + (\sin\theta \cdot K_z)^2}. \tag{7}$$

This equation will be used to approximate the equivalent spring constant the baseplate experiences. Given that the baseplate's velocity is parallel with displacement, one finds the net damping constant as:

$$C_n = \sqrt{(\cos\theta \cdot C_h)^2 + (\sin\theta \cdot C_z)^2}. \tag{8}$$

K_n and C_n represent the soil's spring and damping constants after adjusting for the mortar's baseplate area and launch angle. These will be used in equation (2).

2.4 Baseplate Measurements

Here, we examine the mortar measurements involved. As a reference for typical launch angles, the M252A mortar launches between 45.84°and 86.80°of elevation [15]. Simulations are done for launch angles of 50°, 65°, and 80°.

Typical 60-mm and 120-mm mortars have baseplate diameters of 351 mm and 1100 mm, respectively. A 100% baseplate scale represents the area of the currently manufactured baseplate size. Since we want to investigate the effect of baseplate area on the mortar-ground system, we will also examine a 25% scaled-down baseplate (a 75% scale - that is, 75% of the current area) and a 25% scaled-up baseplate (a 125% scale - 125% of the current area). Table 3 describes the baseplate areas and masses:

	75%	100%	125%	Mass
60-mm	$0.07257\,\mathrm{m}^2$	$0.09676\,\mathrm{m}^2$	$0.1210\,\mathrm{m}^2$	23 kg
120-mm	$0.7127\,\mathrm{m}^2$	$0.9503\,\mathrm{m}^2$	$1.188\,\mathrm{m}^2$	285 kg

Table 3: This table lists the current baseplate area (100%), as well as scaled-down (75%) and scaled-up (125%) areas. Also shown is mortar mass.

These measurements are taken from references [2], [10], [1].

Using equations (7), (8), and Tables 2, 3, we calculated the soil parameters for various soil conditions, various launch angles, and various baseplate areas. These tables are found in Appendix A.

3 Solving The Mortar ODE

Consider equations of the form $mx''(t) + cx'(t) + kx(t) = F(t)$, where $F(t)$ is the non-homogeneous component. This can be solved by using the variation of parameters method.

The general solution, $x_{GS}(t)$, is of the form:

$$x_{GS}(t) = x_{CS}(t) + x_P(t)$$

$x_{CS}(t)$ refers to the *complementary* solution and $x_P(t)$ refers to the *particular* solution. $x_{CS}(t)$ is the solution to $x''(t) + \frac{c}{m}x'(t) + \frac{k}{m}x(t) = 0$, and can be obtained by looking at the corresponding characteristic equation:

$$r^2 + \frac{c}{m}r + \frac{k}{m} = 0. \tag{9}$$

Solving for r yields r_1 and r_2, which are then used to obtain basis solutions $x_1(t) = e^{r_1 t}$ and $x_2(t) = e^{r_2 t}$. Having found $x_1(t)$ and $x_2(t)$, we use the variation of parameters to solve for the particular solution:

$$x_P(t) = -x_1(t)\int \frac{x_2(t)F(t)}{W(t)}\,dt + x_2(t)\int \frac{x_1(t)F(t)}{W(t)}\,dt, \tag{10}$$

where $W(t) = x_1(t)x_2'(t) - x_1'(t)x_2(t)$.

Note that we solved equation (10) symbolically via MATLAB's symbolic math toolbox. That gives us a particular solution in terms of t, as opposed to numerical values.

At the very beginning of the firing process, the baseplate starts at equilibrium. This gives the initial conditions that $x(0) = 0$ and $x'(0) = 0$. Being mindful of Heaviside behavior at $t = 0$, one can use these initial conditions to obtain a specific solution.

We can examine the discriminant to analyze damping behavior. For our mortar system, the discriminant is given by $c^2 - 4mk$. A positive discriminant indicates over-damping, a zero discriminant indicates a critically-damped system, and a negative discriminant indicates under-damping. Using the soil conditions in Appendix A and masses given in Table 3, one finds that each combination of soil condition, launch angle, and baseplate size has a positive discriminant. Hence, mortar baseplate dynamics are an over-damped system, meaning that the system slowly returns to its equilibrium position without oscillations.

4 Recoil Profiles and Simulation Settings

We have now developed a differential equation describing baseplate movement under recoil force, found the recoil, soil, and mortar parameters, and determined the various testing conditions. Next, we proceed to simulate mortar baseplate displacement under various conditions.

All simulations use equations (5) and (6) to model recoil force for 60-mm and 120-mm mortars, respectively. Figures 11a and 11b describes the recoil forces over time. Note that the force is discontinuous, as indicated by the vertical dashed line.

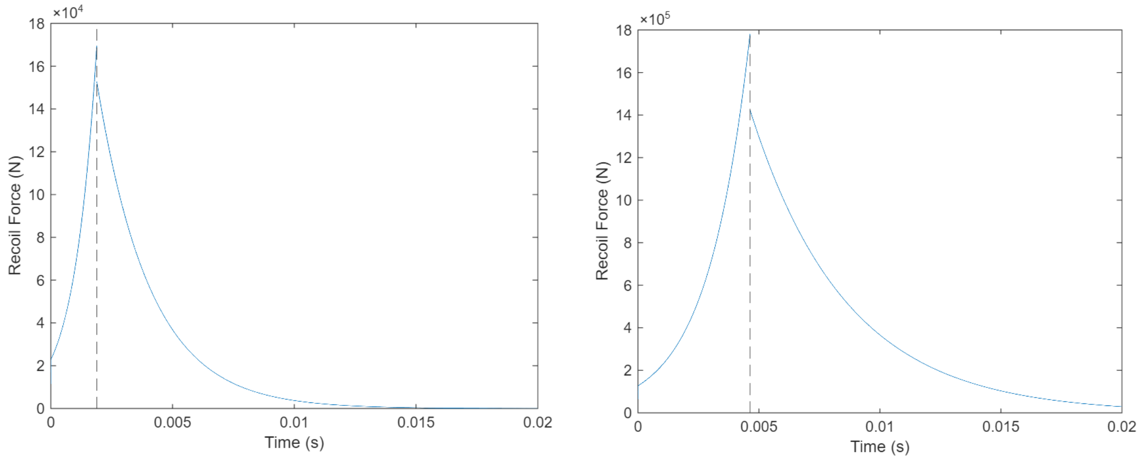

(a) 60-mm mortar.

(b) 120-mm mortar.

Figure 11: The recoil-time plots for 60-mm and 120-mm mortars.

The first simulation determines baseplate sinkage under hard, medium, and soft soil conditions while keeping a 65°launch angle and 100% baseplate scale. This simulation uses soil parameters from Tables 12 and 13.

The second simulation determines baseplate sinkage under 50°, 65°, and 80°launch angles under a medium soil condition and a 100% baseplate scale. This uses the soil parameters from Tables 14 and 15. This particular simulation results in each displacement being along a different axis, making direct comparison unclear. This can be resolved by comparing *vertical* sinkages as well. For a particular displacement under a particular launch angle, one can multiply the displacement graph by the sine of the launch angle to obtain a graph of the vertical sinkage.

The third simulation determines baseplate sinkage under various baseplate areas. This simulation considers sinkage for a baseplate with 75%, 100%, and 125% of the currently manufactured baseplate area. This is done with a 65°launch angle and a medium soil condition, using soil parameters from Tables 16 and 17.

5 Results

This section describes the results particular to each simulation condition. The exact peak displacement, sinkage, and velocities are aggregated in Appendix B. The main results are illustrated in Figures 12, 14, 17.

5.1 Variable Soil Hardness

For both 60-mm and 120-mm mortars, soil hardness significantly influences on baseplate displacement, $x(t)$, and velocity, $x'(t)$. Simulations used the testing parameters in Tables 12 and 13.

The results of the simulation are displayed in Figure 12:

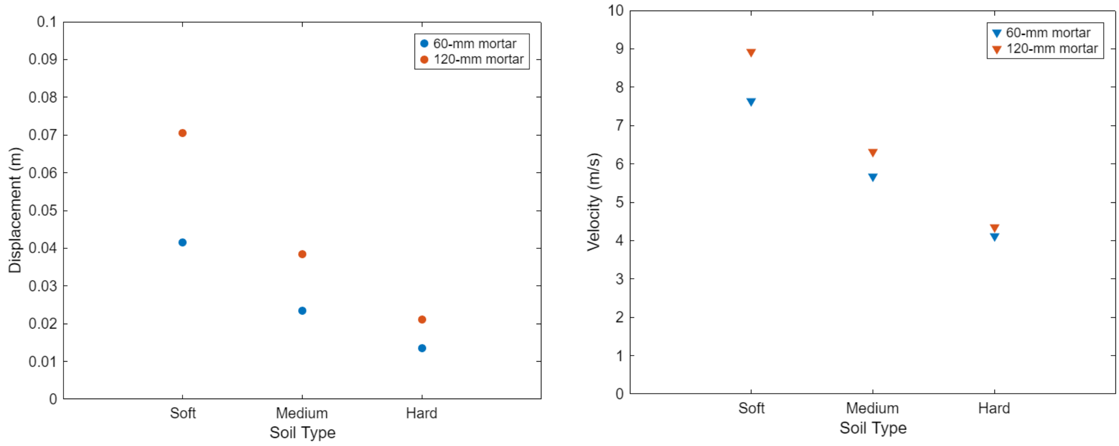

Figure 12: Peak displacement and velocity plots for 60-mm and 120-mm mortars, for various soils.

For 60-mm mortars, the baseplate sank 207.9% deeper in soft soil compared to hard soil. This ratio increased to 234.0% for 120-mm mortars. This sinkage was also at a faster rate; relative to on hard soils, peak velocities in soft soils were 85.78% and 105.4% higher for 60-mm and 120-mm mortars, respectively. The peak displacement also occurs at later times for softer soils. Tables 4 and 5 list the peak displacement and velocity times.

Soil	Peak Displace Times (s)	Peak Velocity Times (s)
Hard	0.006925	0.002557
Medium	0.008671	0.002924
Soft	0.01145	0.003430

Table 4: This table lists peak displacement and velocity times for 60-mm mortars.

Soil	Peak Displace Times (s)	Peak Velocity Times (s)
Hard	0.01101	0.005188
Medium	0.01340	0.005718
Soft	0.01703	0.006480

Table 5: This table lists peak displacement and velocity times for 120-mm mortars.

Observe that the peak displacements and velocities occur later in softer soils. Referencing Tables 12 and 13, this is because softer soils have lower damping and spring constants. As a result, the baseplate must sink deeper and move faster to experience the same resistive force as found in harder soils.

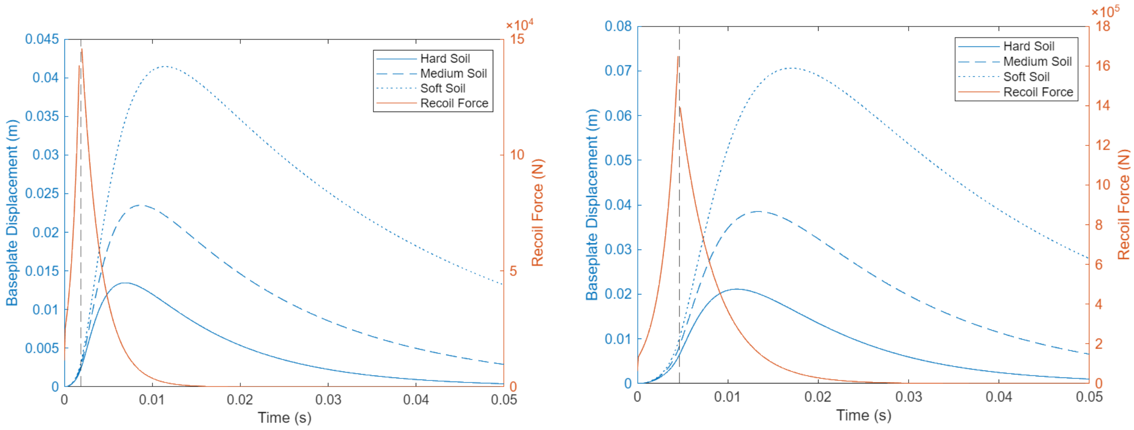

(a) 60-mm mortar

(b) 120-mm mortar.

Figure 13: Displacement-time plots (with recoil) for 60-mm and 120-mm mortars, for various soil hardness.

Figures 13a and 13b describe baseplate displacement (in m) over time (in s) for 60-mm and 120-mm mortars under various soil conditions. Also displayed is the recoil force (in N) for the respective mortars. Observe that in every case, the peak displacement occurs *after* the recoil force has largely decreased.

To determine the velocity, we can simply look at the slope of the displacement-time graphs. At the time of peak velocity (as shown by the steepest increase on the displacement-time graphs), the acceleration of the baseplate is zero. At that specific time, the magnitude of the soil's resistive forces begin to overcome recoil forces and the baseplate's inertia. Because soil resistive forces are defined as acting in the $-x$ direction, the baseplate will experience a negative acceleration. This corresponds with the velocity decrease after the time of peak velocity.

5.2 Variable Launch Angle

For both 60-mm and 120-mm mortars, changing the launch angle has the least effect on baseplate movement. This simulation ran the parameters from Tables 14 and 15. Peak displacement, vertical sinkage, and velocity are presented in Figure 14:

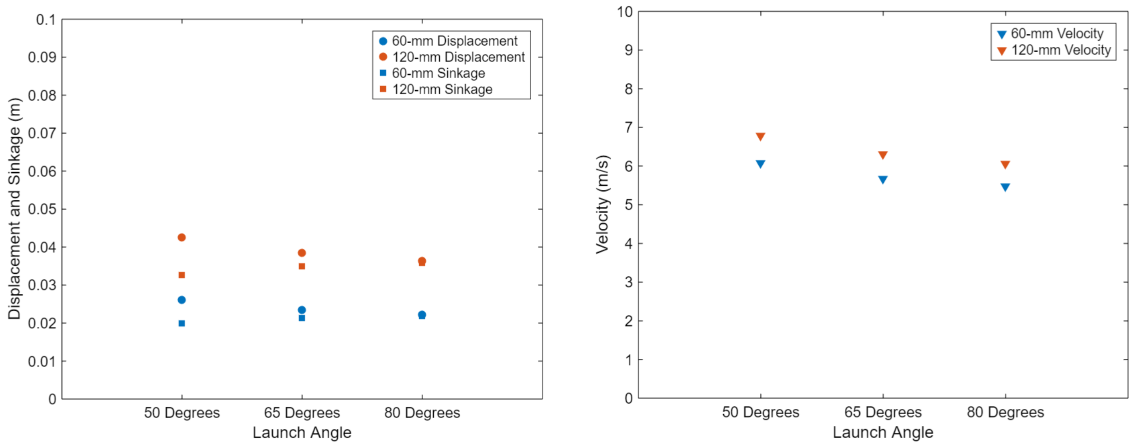

Figure 14: Peak displacement, sinkage, and velocity values for 60-mm and 120-mm mortars, for various launch angles.

Increasing the launch angle from 50°to 80°decreased the displacement by 14.60% and 14.44%, for 60-mm and 120-mm mortars, respectively. Similarly, peak velocity decreases by 9.865% and 10.86%. Note, however, that the displacement for a particular launch angle refers to movement along that particular angle's skewed axis. To provide a common axis on which to compare baseplate sinkage, we examine vertical sinkage.

Vertical sinkage increased because the amount of recoil force acting in the vertical direction increased. However, increases in the vertical component of recoil force are offset by soil's higher damping and spring constants in the vertical direction, as shown in Table 2. As a result, 60-mm and 120-mm mortars experienced only 9.729% and 10.02% increase in vertical sinkage, respectively.

Figures 15a, 15b, 16a, and 16b display baseplate displacement and vertical sinkage over time for 60-mm (left) and 120-mm (right) mortars. As shown in Figures 16a and 16b, differences in vertical sinkage are relatively small compared to differences in displacement. Compared to changes in soil hardness and baseplate area, changes in launch angle appear to have minimal impact on baseplate displacement, vertical sinkage, and velocity.

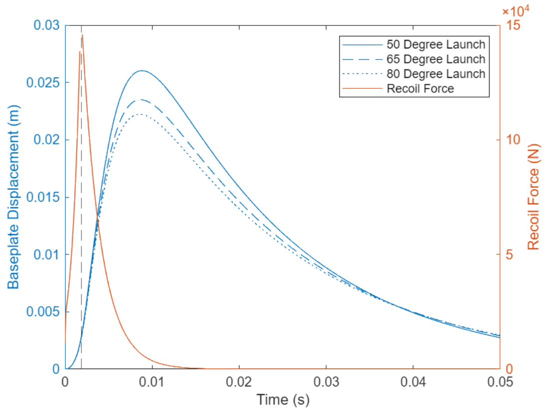

(a) 60-mm mortar.

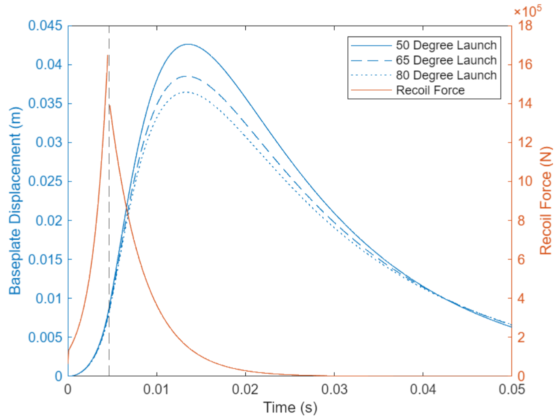

(b) 120-mm mortar.

Figure 15: Displacement-time plots for 60-mm and 120-mm mortars, for various launch angles.

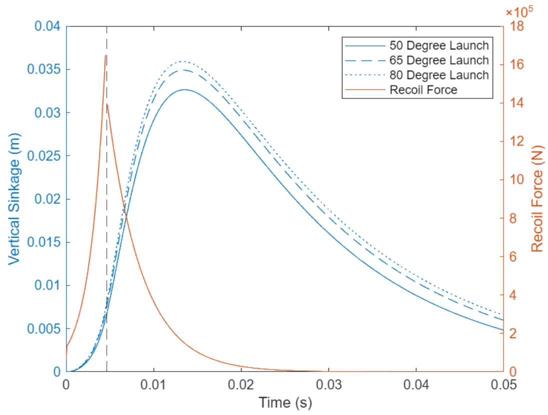

(a) 60-mm mortar.

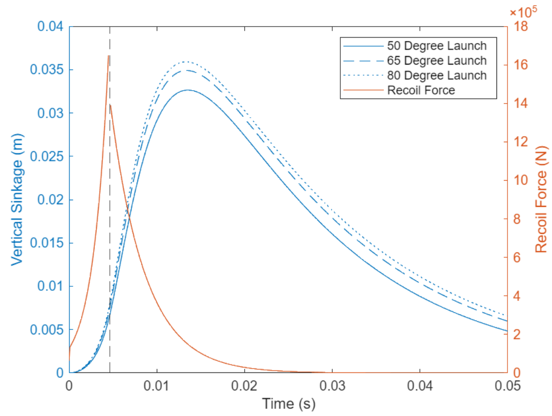

(b) 120-mm mortar.

Figure 16: Sinkage-time plots for 60-mm and 120-mm mortars, for various launch angles.

5.3 Variable Baseplate Area

The third simulation considers baseplate area while maintaining a constant 65°launch angle and medium soil condition. We found that increasing baseplate area significantly reduces displacement. This simulation used the soil parameters from Tables 16 and 17. Figure 17 summarizes the peak displacements and peak velocities when using various sizes of baseplate.

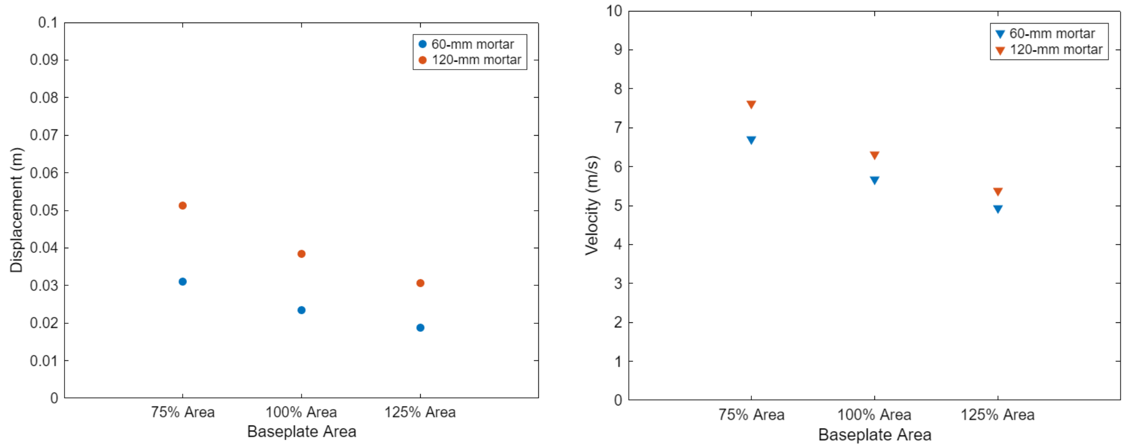

Figure 17: Peak displacement and velocity plots for 60-mm and 120-mm mortars, for various baseplate areas.

Relative to currently manufactured baseplate areas, the 125% scaled baseplate area displaced 19.84% and 20.18% less for 60-mm and 120-mm mortars, respectively. Meanwhile, the 75% scaled baseplate displaced 32.27% and 33.19% deeper, respectively.

Regarding peak velocity, a scale-up to 125% baseplate area reduced peak baseplate velocity by 13.10% and 14.54% for 60-mm and 120-mm mortars. Conversely, a scale-down to 75% area increased peak velocity by 18.15% and 20.85%, respectively.

Analyzing the displacement-time plots, one can see that larger baseplates displace significantly less, at a slower rate, and return to equilibrium faster.

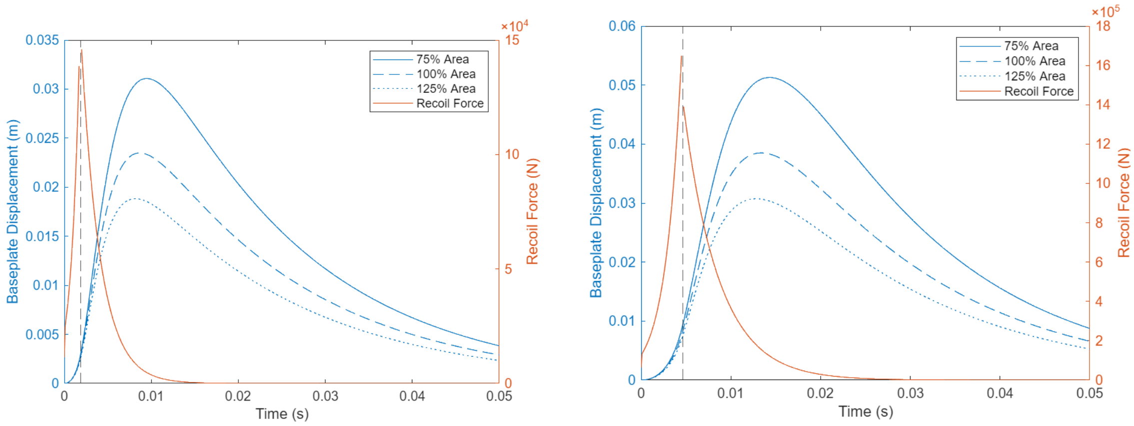

(a) 60-mm mortar.

(b) 120-mm mortar.

Figure 18: Displacement-time plots for 60-mm and 120-mm mortars, for various baseplate areas.

6 Damping Analysis

One can determine the system's damping properties under various soil types, launch angles, and baseplate sizes. This analysis provides additional insight on baseplate kinematics under various conditions. Engineers and physicists analyze the discriminant to design and control spring-mass-damper systems for desired performance. Since this system is over-damped, it slowly returns to equilibrium with no oscillation.

6.1 Damping with Variable Soil Hardness

For a 65°launch condition and 100% baseplate area, Tables 6 and 7 describe the discriminant for 60-mm and 120-mm mortars under various soil conditions. The discriminant of equation (2) is $c^2 - 4mk$.

Soil Condition	Hard	Medium	Soft
Discriminant	$441.6 \cdot 10^6$	$173.3 \cdot 10^6$	$62.54 \cdot 10^6$

Table 6: Discriminant values for a 60-mm mortar, under various soil hardness.

Soil Condition	Hard	Medium	Soft
Discriminant	$37.97 \cdot 10^9$	$14.91 \cdot 10^9$	$5.384 \cdot 10^9$

Table 7: Discriminant values for a 120-mm mortar, under various soil hardness.

Figures 19a and 19b describe the amplitude of the soil's responses to different external forcing frequencies. The positive discriminant values in Tables 6 and 7, as well as the continuous response decrease in Figures 19a and 19b, show that this system is over-damped. Observe that harder soils are more heavily damped.

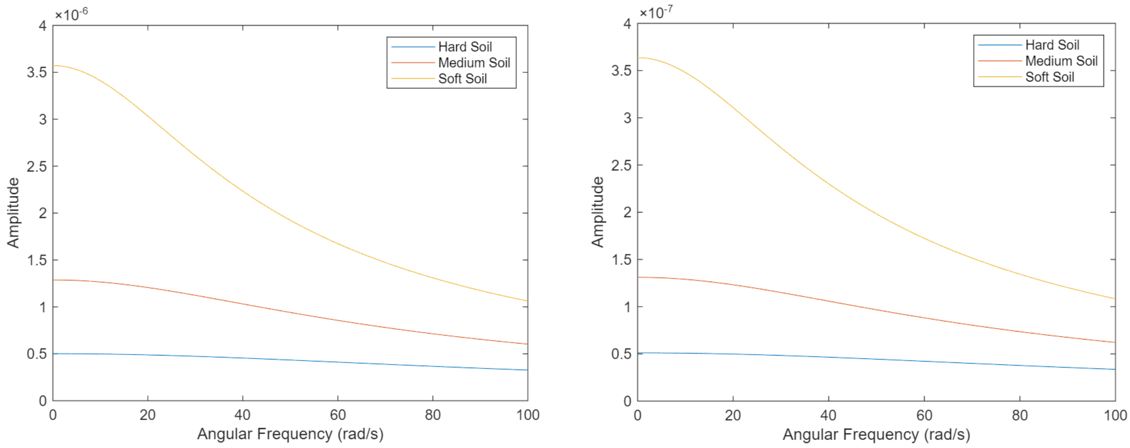

(a) 60-mm mortar.

(b) 120-mm mortar.

Figure 19: Amplitude gain plots for 60-mm and 120-mm mortars, for various soil hardness.

The more over-damped the system, the slower it returns to equilibrium overall. However, in the simulation on variable soil hardness, it appears that harder soils return to equilibrium *earlier* than softer soils. This contradiction can be resolved by noting that harder soils displaced significantly less than softer soils. Harder soils have higher spring and damping constants, leading to more resistance against baseplate displacement and movement. As a result, peak displacement values decrease, reducing the distance the baseplate has to move to return to equilibrium. Additionally, a larger discriminant implies that there is a larger separation of roots r_1 and r_2, where $r_1 = \frac{-c+\sqrt{c^2-4mk}}{2m}$ and $r_2 = \frac{-c-\sqrt{c^2-4mk}}{2m}$, resulting in more rapid initial decay due to one term decaying much faster. This also explains why harder soils began returning to equilibrium sooner than softer soils. Conversely, softer soils have smaller discriminants, leading to a slower initial decay (as seen in the later peak displacement and velocity times).

Besides varying the soil hardness, varying the launch angle and baseplate area will affect over-damping. Referencing Tables 14, 15, 16, and 17, one can examine damping behavior for various launch angles and baseplate areas.

6.2 Damping with Variable Launch Angle

Varying launch angle while maintaining a 100% baseplate area and medium soil, one obtains Tables 8 and 9:

Launch Angle	50°	65°	80°
Discriminant	$126.3 \cdot 10^6$	$173.3 \cdot 10^6$	$203.1 \cdot 10^6$

Table 8: Discriminant values for a 60-mm mortar, under various launch angles.

Launch Angle	50°	65°	80°
Discriminant	$10.47 \cdot 10^9$	$14.91 \cdot 10^9$	$17.73 \cdot 10^9$

Table 9: Discriminant values for a 120-mm mortar, under various launch angles.

Plotting the amplitude gain under various launch angles:

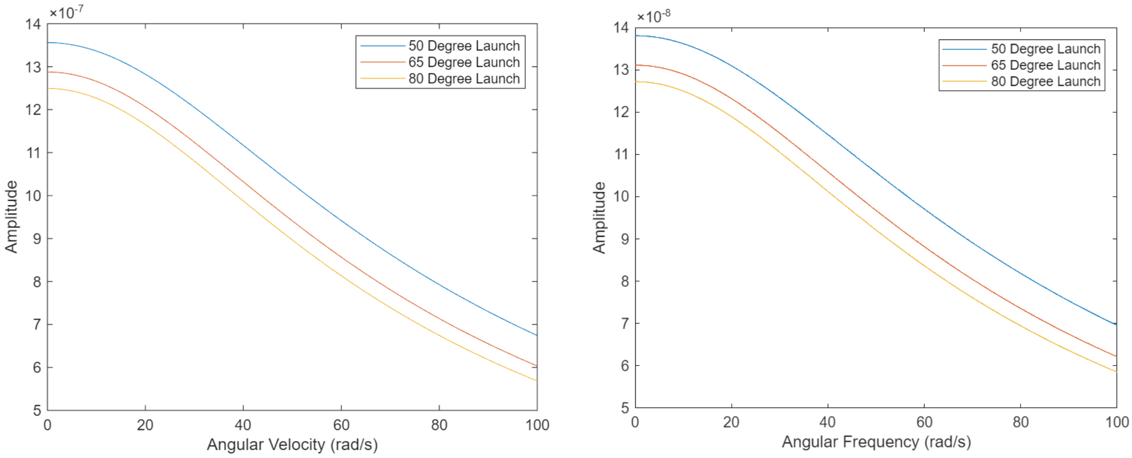

(a) 60-mm mortar.

(b) 120-mm mortar.

Figure 20: Amplitude gain plots for 60-mm and 120-mm mortars, for various launch angles.

One observes that altering the launch angle does not change the discriminant values or gain plot as much as altering the soil hardness.

6.3 Damping with Variable Baseplate Area

Varying baseplate area while maintaining a 65°launch angle and medium soil, one obtains Tables 10 and 11, respectively:

Baseplate Size	75% Area	100% Area	125% Area
Discriminant	$84.07 \cdot 10^6$	$173.3 \cdot 10^6$	$293.1 \cdot 10^6$

Table 10: Discriminant values for a 60-mm mortar, under various baseplate areas.

Baseplate Size	75% Area	100% Area	125% Area
Discriminant	$6.757 \cdot 10^9$	$14.91 \cdot 10^9$	$26.02 \cdot 10^9$

Table 11: Discriminant values for a 120-mm mortar, under various baseplate areas.

Plotting the amplitude gain under various baseplate sizes:

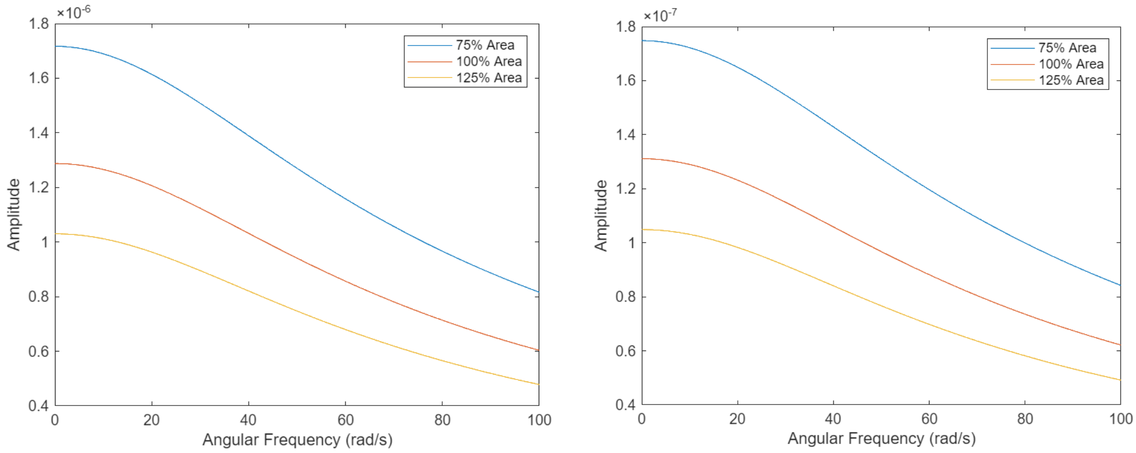

(a) 60-mm mortar. (b) 120-mm mortar.

Figure 21: Amplitude gain plots for 60-mm and 120-mm mortars, for various baseplate areas.

Observe that baseplate size is quite significant in affecting determinant values and gain plots. While altering the baseplate size does not affect the over damping properties as much as altering the soil hardness, damping behavior appears to be more influenced by baseplate size than launch angle.

7 Conclusions

7.1 Findings

This project analyzed the effects of soil hardness, launch angle, and baseplate area on baseplate movement. Regarding soil hardness, baseplate displacement and velocity significantly increased with harder soil. This is because harder soils have higher damping and spring constants that more effectively resist recoil forces. For example, at a launch angle of 65°and 100% baseplate area, launching on hard soil compared to medium soil would decrease sinkage by 42.69% for a 60-mm mortar. This was calculated by taking the difference between the peak displacement on hard (0.01346 m) and medium (0.02349 m), and dividing that quantity by the peak displacement on medium soil. That is:

$$\frac{\textbf{difference in displacement}}{\textbf{medium soil displacement}} = \frac{0.01346 - 0.02349}{0.02349} \cdot 100\% = -42.69\%$$

Launch angle did not significantly influence baseplate movement. For a 60-mm mortar firing on medium soil at a 100% baseplate size, increasing the launch angle from 50°to 80°decreased the peak displacement by 14.60%. However, vertical sinkage increased by only 9.729%. This is because increases in launch angle correspond with increases in soil resistive forces; soil has higher damping and spring constants in the vertical direction. The calculations for these percent figures are below:

$$\frac{\textbf{difference in displacement}}{\textbf{displacement for 50}^\circ\textbf{ launch}} = \frac{0.02222 - 0.02602}{0.02602} \cdot 100\% = -14.60\%$$

$$\frac{\textbf{difference in vertical sinkage}}{\textbf{vertical sinkage for 50}^\circ\textbf{ launch}} = \frac{0.02188 - 0.01994}{0.01994} \cdot 100\% = 9.729\%$$

Finally, increasing baseplate area significantly reduces baseplate movement. As the baseplate area increased, the effective soil damping and spring constants proportionally increased. This is because a larger area will be in contact with more soil. For a 60-mm mortar firing on medium soil at a launch angle of 65°, increasing the original baseplate area by 25% led to a 19.84% decrease in peak displacement. Shown below are the calculations to arrive at this figure.

$$\frac{\textbf{difference in displacement}}{\textbf{displacement for 100\% area}} = \frac{0.01883 - 0.02349}{0.02349} \cdot 100\% = -19.84\%$$

Differences in baseplate displacement and velocity can be attributed to soil's different over-damping behaviors under different conditions. Harder soils have a larger discriminant, meaning that they are more heavily damped compared to softer soils. Increasing baseplate area also increased the level of over-damping; larger baseplate areas have higher discriminants. The discriminant slightly increased with slightly increasing angle, but not to the same extent as increases in baseplate area or increases in soil hardness.

In summary, to minimize baseplate movement (and improve firing accuracy), one should launch on hard soils, at a high angle, with a large baseplate. However, it is important to note that soil conditions depend on battlefield geography. Additionally, launch angle is determined by the where the target is in relation to the mortar. This means that mortar crews may be unable to increase firing accuracy by controlling soil conditions or target location. However, in preparation for military operations, manufacturers *can* increase baseplate size. Then, during firing, the larger area will minimize baseplate sinkage. Therefore, to minimize mortar movement and increase firing accuracy, this paper recommends using the largest baseplate practical.

7.2 Further Research

Soil pressure-sinkage is not linear. Further research could take into consideration this fact and model baseplate displacement with a nonlinear ordinary differential equation. Additionally, this project assumed that the baseplate was placed such that the ground was perpendicular to recoil force. In some cases, however, the baseplate may be placed on flat ground such that the baseplate is *not* perpendicular to recoil force. This would change the effective surface area since the baseplate is resisting recoil and soil properties at a skewed angle.

7.3 Notes

This section will address some of the contradictions encountered during this paper's research process. Sources [4] and [5] used the Bekker model to determine the relationship between applied pressure and soil sinkage. This could be translated into a soil spring constant. However, this relationship may be nonlinear. While using the Bekker model may have increased accuracy, it would lead to a nonlinear model for baseplate movement, making it harder to solve. Meanwhile, reference [7] showed the relationship between pile-driving velocity and resistive force in clay soils. From this, one could obtain a damping coefficient. While the relationship between resistance and velocity was approximately linear, it was unclear if the experimental setup was comparable to a mortar. This is because reference [7] involved *penetrating* a soil sample with a metal rod, while mortar baseplates only *compact* the soil. Soil damping and spring constants were pulled from reference [11] instead.

Additionally, pressure and mortar measurements for this paper's 60-mm and 120-mm mortars were measured from different models of mortars. Source [3] gave the barrel pressure profile for an undisclosed model of 60-mm mortar, launching an unknown type of shell. Assuming that each model of 60-mm mortar is roughly similar in design, this paper considered the median mass and baseplate measurements in reference [2] to be similar to the undisclosed mortar measured in reference [3]. Regarding pressure and mortar measurements for 120-mm mortars, pressure-time profiles of the 120 KRH 92 mortar were taken from reference [12]. The 120 KRH 92 mortar was specified to be 285 kilograms [10]. However, the baseplate diameter was unavailable. The 120-mm M12 mortar's baseplate diameter (from reference [1]) was used in place. The shells launched were specified to be either high-explosive (HE) rounds or ballistic slugs. Note that the "explosive" in HE refers to the impact with the target, not the launch.

Appendix A. Simulation Parameter Tables

Below are the soil parameters used in this project's simulations

Variable Soil Hardness Parameters

Tables 12 and 13 describe the soil parameters for a 65°launch angle and 100% of baseplate size:

Soil Condition	Hard	Medium	Soft
K_n, N/m	$1.993 \cdot 10^6$	$776.7 \cdot 10^3$	$278.0 \cdot 10^3$
C_n, N·s/m	$25.00 \cdot 10^3$	$15.64 \cdot 10^3$	$9.397 \cdot 10^3$

Table 12: Soil parameters for a 60-mm mortar.

Soil Condition	Hard	Medium	Soft
K_n, N/m	$19.57 \cdot 10^6$	$7.628 \cdot 10^6$	$2.750 \cdot 10^6$
C_n, N·s/m	$245.5 \cdot 10^3$	$153.6 \cdot 10^3$	$92.30 \cdot 10^3$

Table 13: Soil parameters for a 120-mm mortar.

Variable Launch Angle Parameters

Tables 14 and 15 describe the soil parameters for medium soil and 100% of baseplate size:

Launch Angle	50°	65°	80°
K_n, N/m	$737.5 \cdot 10^3$	$776.7 \cdot 10^3$	$800.5 \cdot 10^3$
C_n, N·s/m	$13.93 \cdot 10^3$	$15.64 \cdot 10^3$	$16.64 \cdot 10^3$

Table 14: Soil parameters for a 60-mm mortar.

Launch Angle	50°	65°	80°
K_n, N/m	$7.243 \cdot 10^6$	$7.628 \cdot 10^6$	$7.861 \cdot 10^6$
C_n, N·s/m	$136.9 \cdot 10^3$	$153.6 \cdot 10^3$	$163.4 \cdot 10^3$

Table 15: Soil parameters for a 120-mm mortar.

Variable Baseplate Area Parameters

Tables 16 and 17 describe the soil parameters for a 65°launch angle and medium soil:

Baseplate Area	75% Area	100% Area	125% Area
K_n, N/m	$582.5 \cdot 10^3$	$776.7 \cdot 10^3$	$970.6 \cdot 10^3$
C_n, N·s/m	$11.73 \cdot 10^3$	$15.64 \cdot 10^3$	$19.56 \cdot 10^3$

Table 16: Soil parameters for a 60-mm mortar.

Baseplate Area	75% Area	100% Area	125% Area
K_n, N/m	$5.721 \cdot 10^6$	$7.628 \cdot 10^6$	$9.535 \cdot 10^6$
C_n, N·s/m	$115.2 \cdot 10^3$	$153.6 \cdot 10^3$	$192.1 \cdot 10^3$

Table 17: Soil parameters for a 120-mm mortar.

Appendix B. Results Tables

Below are tables describing the resulting peak times, displacements, sinkages, and velocities of the simulations.

Variable Soil Hardness Results

Tables 18 and 19 describe the peak displacements and velocities for a 65°launch angle and 100% of baseplate size:

Soil Condition	Displacement (m)	Velocity (m/s)
Hard	0.01346	4.107
Medium	0.02349	5.678
Soft	0.04144	7.630

Table 18: Results for a 60-mm mortar.

Soil Condition	Displacement (m)	Velocity (m/s)
Hard	0.02114	4.339
Medium	0.03850	6.306
Soft	0.07061	8.912

Table 19: Results for a 120-mm mortar.

Variable Launch Angle Results

Tables 20 and 21 describe the peak displacements, sinkages, and velocities for a 65°launch angle and medium soil:

Launch Angle	Displacement (m)	Sinkage (m)	Peak Velocity (m/s)
50°	0.02602	0.01994	6.072
65°	0.02349	0.02129	5.678
80°	0.02222	0.02188	5.473

Table 20: Results for a 60-mm mortar.

Launch Angle	Displacement (m)	Sinkage (m)	Peak Velocity (m/s)
50°	0.04260	0.03263	6.793
65°	0.03850	0.03490	6.306
80°	0.03645	0.03590	6.055

Table 21: Results for a 120-mm mortar.

Variable Baseplate Area Results

Tables 22 and 23 describe the peak displacements and velocities for a 65°launch angle and medium soil:

Baseplate Area	Displacement (m)	Peak Velocity (m/s)
75%	0.03107	6.708
100%	0.02349	5.678
125%	0.01883	4.934

Table 22: Results for a 60-mm mortar

.

Baseplate Area	Displacement (m)	Peak Velocity (m/s)
75%	0.05128	7.621
100%	0.03850	6.306
125%	0.03073	5.389

Table 23: Results for a 120-mm mortar.

Distribution Statement

PA Number: USAFA-DF-2025-49 *"The views expressed in this article, book, or presentation are those of the author and do not necessarily reflect the official policy or position of the United States Air Force Academy, the Air Force, the Department of Defense, or the U.S. Government."*

References

[1] *120 mm System*. 2017. URL: hds.hirtenberger.com/wp-content/uploads/HDS_120mm_System_01-24_red.pdf.

[2] *60 mm Smooth Bore System*. 2017. URL: hds.hirtenberger.com/wp-content/uploads/HDS_60mm_System.pdf.

[3] Grzegorz et. al. "The Use of Geotechnical Methods to Determine the Deformation Parameters of the Ground in Terms of Operation and Safety of Mortar Use". In: *Materials* 14.23 (2021). DOI: http://dx.doi.org/10.3390/ma14237237.

[4] Pan et. al. "Construction and Experimental Verification of Sloped Terrain Soil Pressure-Sinkage Model". In: *Agriculture* 11.3 (2021). DOI: https://doi.org/10.3390/agriculture11030243.

[5] Salman et. al. "Design and performance evaluation of bevameter equipment". In: *Journal of Advanced Mechanical Design, Systems, and Manufacturing* 14.6 (2020). DOI: https://doi.org/10.1299/jamdsm.2020jamdsm0084.

[6] British Army. *Equipment: Small Arms and Support Weapons*. URL: army.mod.uk/equipment/small-arms-and-support-weapons/.

[7] A Benamar. "Pile Behavior during Driving". In: *International Society for Soil Mechanics and Geotechnical Engineering* (1999).

[8] *Encyclopaedia Britannica*. 12th. Vol. 32. New York, NY: The Encyclopaedia Britannica Company, 1922.

[9] The Editors of Encyclopaedia Britannica. *Mortar*. URL: britannica.com/technology/mortar-weapon.

[10] *Finnish 120 KRH 92 mortars used by Ukrainian army — OSINT researchers*. 2022. URL: mil.in.ua/en/news/finnish-120-krh-92-mortars-used-by-ukrainian-army-osint-researchers/.

[11] Anand M. Gharad and Ranjan S. Sonparote. "Evaluation of vertical impact factor coefficents for continuous and integral railway bridges under high-speed moving loads". In: *Earthquake Engineering and Engineering Vibration* 20.2 (2021). DOI: https://doi.org/10.1007/s11803-021-2034-7.

[12] Seppo Moilanen Juha Toivola and Henna-Riitta Jussila. "Force, pressure and strain measurements for traditional heavy mortar launch cycle". In: *Rakenteiden Mekaniikka (Journal of Structural Mechanics)* 44.4 (2011), pp. 309–329.

[13] K. L. Kosanke and L. Weinman. "Typical Mortar Recoil Forces for Spherical Aerial Shell Firings". In: *Fireworks Business* 242 (2004).

[14] *Mortars*. Washington, DC: Headquarters, Department of The Army and The Air Force, 2002.

[15] *Mortars*. Washington, DC: Headquarters, Department of The Army, 2017.

[16] Ankit Rohatgi. *WebPlotDigitizer*. 2024. URL: automeris.io.